The sensory representation of causally controlled objects

Kelly B. Clancy[1] and Thomas D. Mrsic-Flogel[1]

1. Sainsbury Wellcome Centre, UCL, 25 Howland Street London, W1T 4JG, UK

Correspondence: Kelly Clancy (k.clancy@ucl.ac.uk) and Thomas Mrsic-Flogel (t.mrsic-flogel@ucl.ac.uk)

Abstract

Intentional control over external objects is informed by our sensory experience of them, in a continuous dialogue between action and perception. How such control is represented at the sensory level, however, is not understood. Here we devised a brain machine interface (BMI) task that enabled mice to guide a visual cursor to a target location for reward, using activity in brain areas recorded with widefield calcium imaging. Parietal and higher visual cortical regions were more engaged when expert animals controlled the cursor, but not in naïve mice learning the task. Intentional control enhanced responses: single-cell recordings from parietal cortex indicated that the same visual cursor elicited larger responses when mice controlled it than when they passively viewed it. Moreover, neural responses were greater when the cursor was moving towards the target than away from it. Thus, the sensory representation of a causally-controlled object is sensitive to a subject's intention, as well as the object's instantaneous trajectory relative to the subject's goal: potentially strengthening the sensory feedback signal to adjudicating areas for exerting more fluent control.

Introduction

The experience of agency is integral to our sense of self and responsibility, and its dysfunction in a number of psychopathologies can have devastating social effects (Haggard, 2017). But how is an internal locus of control represented in the brain? How does the brain infer a causal relationship between its activity and the sensed world, and how does this affect the sensory encoding of controlled external objects? Actions and perceptions reciprocally affect one another (Dewey, 1896). The sense of agency can be operationalised to inferring a causal relationship between a subject's internally generated actions or activity, and their outcome in the external world. In motor learning, for example, the relationship between an action and its outcome can be learned and re-learned throughout adulthood as animals acquire new motor skills. Brain machine interfaces (BMI) are a method for investigating how subjects learn arbitrary action-outcome relationships (Fetz, 1969; Bakay and Kennedy, 1998; Nicolelis, 2001; Donoghue, 2002; Carmena et al., 2003; Sitaram et al., 2017). When learning to control a BMI, animals employ the same mechanisms as implicated in motor learning (Koralek et al., 2012; Neely et al., 2018). But unlike motor learning, wherein animals learn a task and researchers must search for correlates of the behaviour in patterns of neural activity, BMIs allow the experimenter to precisely control sensory feedback, as well as prescribe the requisite activity patterns necessary for successful task execution, which can then be changed day to day. Thus, animals learning neuroprosthetic control of external objects must engage in continuous self-monitoring to assess the contingency between their neural activity and its outcome, preventing them from executing a habitual or fixed motor pattern.

A key aspect of self-monitoring is the sensory feedback from the object being controlled by the agent. Yet little is known about how causally controlled objects are represented in the brain. Studies have implicated parietal cortex in intention, as well as the subjective assessment of agency over outcome. Disrupting activity

in parietal cortex with TMS temporarily ablates self-reported agency (Chambon et al., 2015), and parietal activity has been found to be involved in representing task rules, the value of competing actions, and visually-guided real-time motor plan updating (Andersen et al., 1997; Pisella et al., 2000; Sugrue et al., 2004; Kahnt et al., 2014; Wisniewski et al., 2015). Motor plans can be decoded from parietal activity, and its responses are task-, expectation-, and goal-dependent (Andersen and Cui, 2009; Aflalo et al., 2015; Licata et al., 2017; Pho et al., 2018; Mohan et al., 2018). All of this evidence suggests that parietal cortex plays a role in intentional, goal directed behaviours. However, previous studies of the role of parietal cortex in intention have not examined how causal control transforms sensory representations across different sensorimotor contingencies.

To address this, we devised a mouse model of adaptive causal control, which allowed us to record from the dorsal cortex of behaving mice while simultaneously recording from individual cells in a mouse homologue of parietal cortex (PPC). Animals learned to guide a visual feedback cursor to a target location in order to obtain a reward using activity in brain areas recorded with widefield imaging. We found evidence that PPC was engaged when expert animals controlled the BMI. We targeted single-cell recordings to this area, and found that the visual cursor elicited larger responses when an animal was controlling it in a closed-loop configuration than when passively viewing it in an open-loop (Bagur et al., 2018). Responses were highest when the cursor was closest to the target zone. Responses were also sensitive to the cursor’s instantaneous trajectory, and were greater when the cursor was moving towards the target than away from it. Thus, the sensory representation of the object was sensitive to the subject's intention, as well as its perception of the object's instantaneous trajectory with respect to its goal. Given that animals have to relearn a changing sensorimotor contingency on the fly, the heightened sensory representation of the cursor at the target position may serve to strengthen the signal to adjudicating areas for informing fluent control over external objects.

Results

Goal-directed control of a visual cursor using areal signals

In order to investigate how causal control over external objects is effected and encoded in mammalian cortex, we trained mice to control a visual feedback cursor using real-time calcium signals recorded with wide-field imaging (largely reflecting the summed spiking activity of local cells (Makino et al., 2017; Clancy et al., 2019). We imaged the dorsal cortex in transgenic mice expressing the calcium indicator GCamp6s in CaMKII+ pyramidal neurons (Wekselblatt et al., 2016), assigning two small frontal regions to control a visual feedback cursor (Figure 1a), similar to a task described previously (Clancy et al., 2014; Koralek et al., 2012). The animal's goal was to bring a visual cursor (presented to both eyes on two separate monitors) to a target position in the centre of its visual field, which they could do by increasing activity in control region 1 (R1) relative to control region 2 (R2, see Methods). In this way, animals could not achieve the target by non-specifically increasing or decreasing activity. Regions were usually placed over ipsilateral motor areas and were changed day to day. The feedback cursor could take one of eight positions on the monitor (Figure 1a), and the cursor had to be held at the target for 300 milliseconds to count as a hit. When animals succeeded in holding the cursor at the target position, a soyamilk reward was delivered after a one second delay. If animals failed to bring the cursor to the target position within 30 seconds, the trial was considered a miss, and a white noise miss-cue was played, followed by a brief time out. Chance performance was assessed using spontaneous activity recorded before the task began, and represents the estimated hit rate the animal would achieve from spontaneous fluctuations of neural signals alone. Animals improved their performance over training (Figure 1b, n = 7 mice), and took less time to reach a criterion performance of 50% correct trials over days (Figure 1c). Control regions could be changed from day to day or within a session, and hit rates improved over time within a session, and after control regions were changed, indicative of learning (Figure 1d).

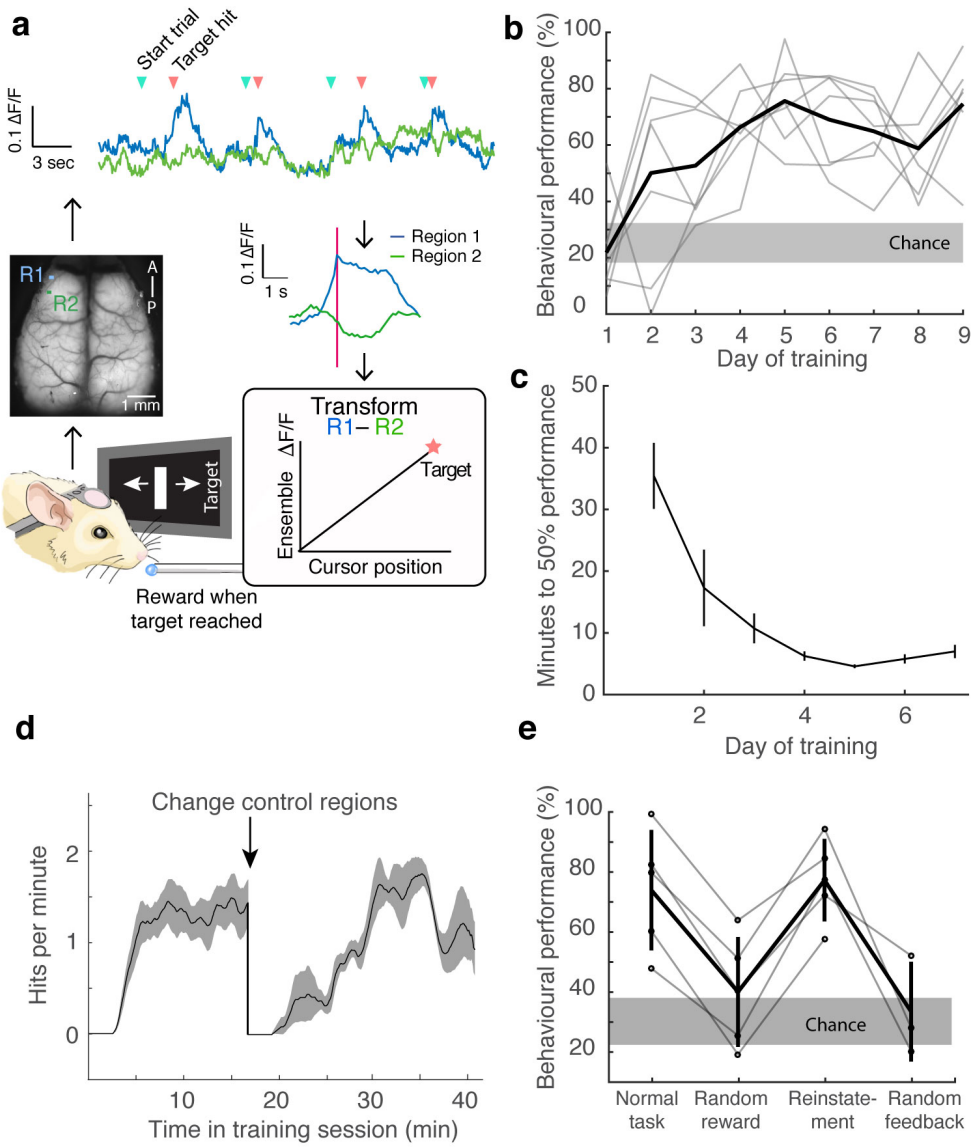

Figure 1. Animals learn to control a visual cursor using areal neural activity
a. Task schematic. Widefield signals were imaged from head-fixed animals in real time and transmuted into the position of a visual cursor. Two regions were used for controlling the cursor, whose activity opposed one another. **b.** Performance (the percentage of trials the animal reached the target) increased above chance over the course of days. Shaded region denotes chance, s.e.m., 7 mice. **c.** Animals achieve 50% performance faster over the course of training (moving average of the number of times the animal reached the target per attempt). **d.** Average hits per minute increased over the course of a session, and recovered within minutes when control regions were changed (n = 7 mice on one day of training, shading denotes s.e.m.). **e.** Performance dropped to near chance when rewards were given randomly, but recovered when target-reward was coupled on a subsequent day (n = 5 mice). Performance also dropped to chance when the visual feedback cursor was uncoupled from neural activity and presented at random (n = 3 mice), even though animals could still achieve reward using the previously learned activity pattern.

To test if the behaviour was goal-directed, we dissociated the reward from the target position. On day 8 of training, animals were allowed to perform the task as usual, but the training session was constrained to 30 minutes. Thereafter, the visual feedback was coupled to the animal's neural activity as before, but the reward was given randomly, at the same rate as an animal performing at average levels. The animals' target hit rate dropped to chance, indicating that the behaviour was goal-oriented (Figure 1e). The fluorescence signals representing the difference between R1 and R2 increased over a normal training session, indicative of increased efficacy of control, and decreased when reward was randomised, again suggesting that animals were effecting the requisite neural patterns in a goal-directed manner (Supp. Figure 1). Animals were able to recover their performance following reinstatement of the normal task on the next day of training (Figure 1e). For a subset of animals, the visual feedback was then randomised: the visual stimulus was presented at random, though animals could still achieve the target with the appropriate neural activity patterns. The animals' ability to bring the cursor to the target dropped to chance levels without meaningful visual feedback (Figure 1e). Animals could perform the task without overt movements, licking, or eye saccades (Supp. Figure 2). Together, this suggests that animals performed the task in a goal-directed, visual feedback-dependent manner, using neural activity alone.

Exploration and exploitation in neural activity space

As control regions were changed day-to-day, the activity patterns necessary for successful BMI control had to be re-learned each session. Example fluorescence traces from control regions indicate the areas were initially highly spontaneously correlated (Figure 2a, top trace). Early in the training session, hits were preceded by diverse activity patterns (Figure 2a, middle trace). By late in the training session, the patterns were consistent (Figure 2a, bottom trace, Supp. Figure 3a), suggesting that animals first explored different activity patterns in order to achieve hits, then exploited the successful pattern to reliably reach the target. Animals

found different ways to do this, sometimes by sweeping activity through R1 towards R2, or by depressing R2 while activating R1 (Supp. Figure 3b). The variance in R1 and R2 activity peaked around hits early in a training session as animals explored strategies that would yield reward. This variance decreased later in the session as animals discovered reliable, reproducible strategies (Supp. Figure 4a, b).

In order to achieve the target activity pattern, animals had to functionally decorrelate the two control regions, which were usually highly spontaneously correlated. Indeed, activity in dorsal cortex was globally correlated in animals pre-task, as indicated by correlation maps using R1 and R2 as seed pixels (Figure 2b, 2a top trace). Although activity in dorsal cortex was globally correlated in animals pre-task, as indicated by correlation maps using R1 and R2 as seed pixels, correlations between these areas decreased during task performance (Figure 2b, Supp. Figure 3c-e). They could arbitrarily decorrelate different regions: in a separate subset of animals trained using an auditory instead of visual feedback cursor, animals could decorrelate visual control areas (Supp. Figure 3d). Interestingly, the task-induced correlation patterns were invariably bilateral, even when control regions were ipsilateral to each other.

Animals took longer to reach criterion 50% performance when control regions were spontaneously highly correlated (Figure 2c). Early in the session, the spectral entropy of activity (a measure of the spectral power distribution of a signal, and a proxy for its complexity, see Methods) around the control regions increased as animals explored activity patterns that would yield reward, then dramatically dropped as they discovered successful patterns and reliably exploited them (Figure 2d). At the start of a session, or when control regions were changed, animals faced with uncertain task rules ‘explored’ activity space through stochastic bursting, and gradually switched to effecting stereotyped patterns they could reliably exploit after having probed the rules of their environment (Tervo et al., 2014).

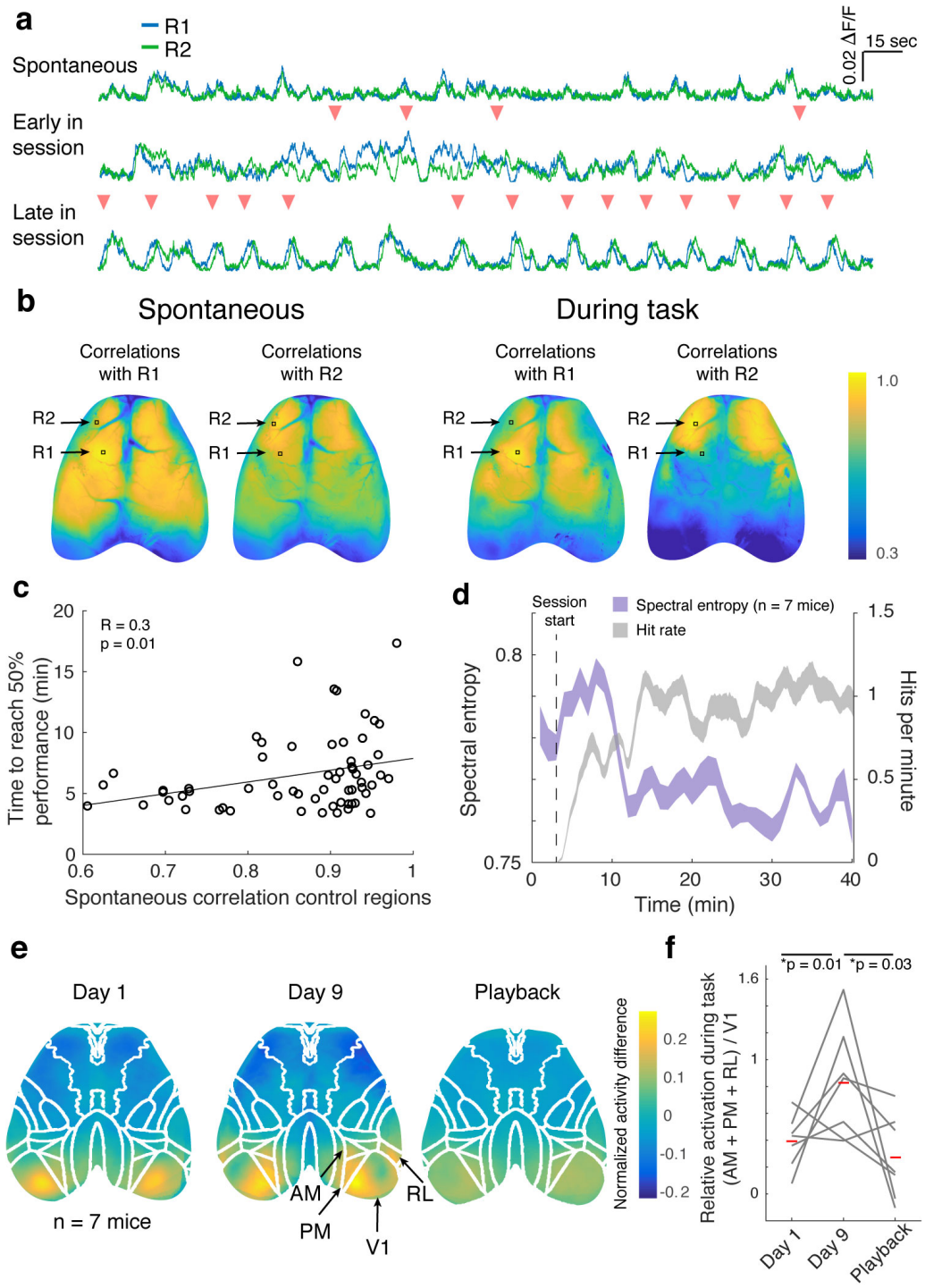

Figure 2. Exploration and exploitation of neural activity patterns
a. Areal signals were highly spontaneously correlated before the training session (top trace). Animals explored different activation patterns early in the training session (middle trace) in order to discover and exploit successful patterns by the end of the session (bottom trace). Pink triangles denote target hits. **b.** Correlation map across cortex with R1 and R2 seeds for spontaneous activity (left) and during task (right). **c.** Animals took longer to reach criterion performance (50% hits/attempt) if control regions were highly spontaneously correlated (data from 7 mice, 9 days of training starting on day 4). **d.** Early

in the session, neural activity around the control regions had high spectral entropy as animals used stochastic bursts of activity to explore the neural patterns that would yield reward. By late in the session, animals had discovered a successful activity pattern to exploit, and spectral entropy in control area activity decreased. Shaded area indicates 95% confidence interval around mean. **e.** Activation map during task on day 1, day 9, and during passive playback of a previous session (normalised activity difference for task-on vs. task-off periods). **f.** The relative ratio of task-activation in higher visual areas versus V1 increased over training. When animals passively viewed playback of the same session, higher areas were not activated. Red bars indicate mean ratios (paired t-test).

Expert performance correlated with increased activity in higher visual areas

We sought to determine what cortical areas were most active during task performance, and how this changed over learning. On the first day of training, primary visual cortex was most active during the task, but as animals became expert in the task, higher visual areas were recruited (Figure 2e-f): in particular, anteromedial cortex (AM), posteriomedial cortex (PM), and rostrolateral visual cortex (RL), similar to previous studies of learning visually-guided tasks in mice (Wekselblatt et al., 2016; Orsolic et al., 2019). Areas AM and RL are considered parietal cortex homologues in mouse cortex (Licata et al., 2017; Mohan et al., 2018; Pho et al., 2018). Activity in these higher areas was not evident in animals passively watching playback of the task stimuli, suggesting their recruitment was specific to goal-oriented task engagement (Figure 2c). A separate cohort of animals trained using an auditory feedback cursor had variable task-active areas (Supp. Figure 5, n = 4 mice), but, as with the visual task, higher activity was also seen in RL.

Population tuning of neurons shifted towards target position

Having identified brain areas implicated in BMI control, we recorded spiking from individual cells while animals performed the task, in order to investigate the task-dependent increase in calcium signals with cellular resolution. We chose to record from functionally identified, parietal homologue area AM, due to its recruitment over learning, and used multi-channel silicon probes to record spikes from individual neurons while simultaneously imaging the rest of dorsal cortex (see

Methods, (Xiao et al., 2017; Clancy et al., 2019; Barson et al., 2018; Peters et al., 2019)). We obtained 16-49 single units per recording, spanning all cortical layers. Units could be classified as regular-spiking (RS) or fast-spiking, putative interneurons (FS) depending on spike width (see Methods, Figure 3a). We recorded from 126 units in 7 mice performing the task (Figure 3b), and 133 units from the same animals passively viewing a playback of a previous session's stimuli. During the task, population firing was significantly increased for stimuli closer to the rewarded stimulus location, and this was true both of FS and RS units (Figure 3d-h, Supp. Figure 6). Responses were also different depending on the preceding stimulus—the firing to stimuli closest to the target was higher if the cursor swept towards the target, but lower if the cursor swept away from it. The opposite was true for the stimuli farther from the target: firing was higher if the cursor swept away from the target.

The target-dependent increased spiking could not be explained by reward expectation, as a subset of animals were given reward at the target position during passive playback as well (Supp. Figure 7). Pupil diameter and locomotion were significantly decorrelated during task performance compared to playback (Supp. Figure 8), suggesting distinct mechanisms underlie pupil size in the two conditions. At the population level, firing rates were uncorrelated with both pupil diameter and pupil position during the task, while firing rates were weakly correlated with pupil diameter during playback (Supp. Figure 8).

We correlated the spike trains of individual units with fluorescence activity across the brain to build affiliation maps for each unit (Xiao et al., 2017; Clancy et al., 2019; Barson et al., 2018; Peters et al., 2019). We aligned these maps to the common coordinate framework of the Allen Brain Atlas using stereotaxic marks on the skull, and sorted these maps by units' preference for different cursor locations. During task performance, the cells most responsive to the target and target-adjacent stimuli were significantly more correlated with activity across the dorsal cortex. This could mean that the boosting around target might be the result of a

cortex-wide signal, or that units tuned to the target correlate more strongly with the rest of dorsal cortex during task performance, but not playback (Supp. Figure 9).

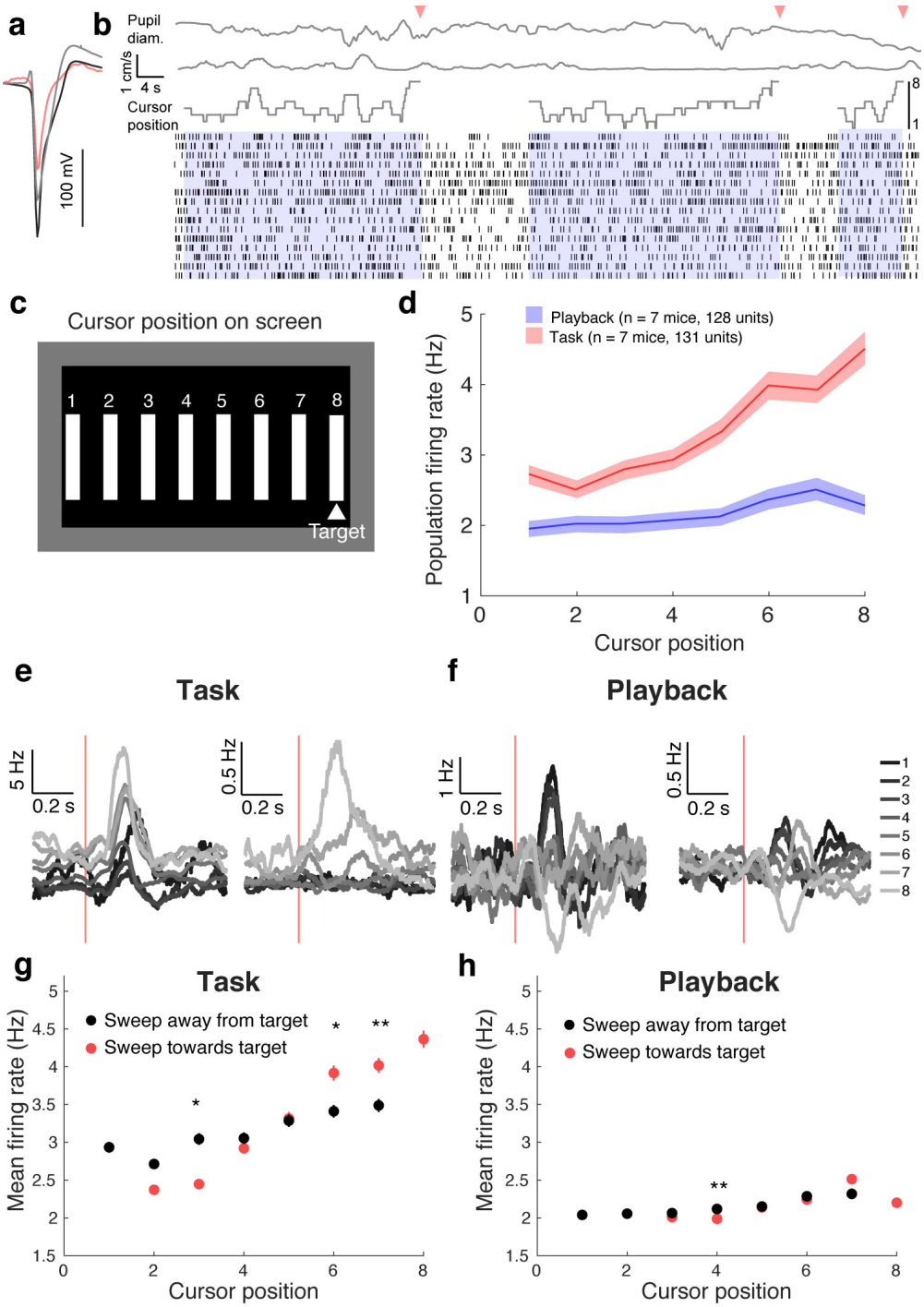

Figure 3. Stimulus tuning shifts to target location and is influenced by sweep direction

a. Example waveforms from three isolated units (FS unit in red). **b.** Example spiking during three successful trials (trials denoted in blue, hits denoted with pink triangle). Top traces are running velocity, pupil diameter and cursor position, from top to bottom. **c.** Feedback schematic: cursor can take one of 8 potential positions on screen**. d.** Average firing rates

for each cursor position during task (red) and playback (blue). Shaded regions indicate 95% confidence interval. **e.** Responses to visual stimuli at the 8 monitor positions for 2 units during task performance (red line indicates stimulus start). **f.** Same as e, for 2 units during playback. **g.** Mean firing rate to different stimuli depended on whether the preceding stimulus was sweeping towards (red) or away (black) from the direction of the target during task (t-test, Bonferroni corrected, asterisks indicate $p>0.05$). **h.** Cursor sweep direction had little effect on firing rates when animals were passively viewing playback.

Discussion

The idea of representation is fundamental to the idea of computation, and the cortex appears to operate on hierarchies of transformed representations. It has become increasingly clear that cortical sensory representations are not strictly veridical reproductions of the outside world, however, but are shaped by a subject's internal states and goals. We sought to understand how having causal control over an external object affects the cortical sensory representation of that object, given that fluent control must be informed by a dialogue between action and perception (Haggard, 2017). Animals learned to causally control an external object using neural calcium signals recorded by widefield imaging, and did so by discovering and exploiting arbitrary mappings between their neural activity and visual feedback that led to reward. This technique enabled us to identify cortical areas involved in task performance, in order to target recordings from individual cells in these areas while animals were engaged in the task. We found that regions of the PPC were recruited during expert BMI control, and that single units in PPC encoded the same visual stimuli differently depending on whether the animal was causally controlling it, or passively viewing it. These results lends further evidence to the idea that PPC activity encodes a subject's intention and self-monitoring of sensorimotor transformations (Andersen and Buneo, 2002; Andersen and Cui, 2009; Desmurget et al., 2009; Aflalo et al., 2015; Cui, 2016).

Previous work indicates that subjects can learn to control neuroprosthetic devices using single cells or bulk electrophysiological signals (Fetz, 1969; Bakay and Kennedy, 1998; Nicolelis, 2001; Serruya et al., 2002; Carmena et al., 2003; Weiskopf et al., 2003; Sitaram et al., 2007; Koralek et al., 2012; Hochberg et al.,

2012; Collinger et al., 2013; Clancy et al., 2014; Sadtler et al., 2014; Prsa et al., 2017; Sitaram et al., 2017; Trautmann et al., 2019), but this is the first work, to our knowledge, to employ control using imaged population calcium signals. This technique allowed us to monitor much of the dorsal cortical network as animals learned neuroprosthetic control, whereas previous BMI work has been limited to recording from neighbouring neurons (Koralek et al., 2012; Clancy et al., 2014; Sadtler et al., 2014; Prsa et al., 2017). Using population signals, rather than individual neurons, to manipulate neuroprosthetic devices might afford more stable and minimally invasive control, robust to losing signals from single control cells.

In order to learn the arbitrary action-outcome relationships required to perform BMI tasks, animals must match internally generated actions or activity with external sensory feedback. To probe how animals learned these contingencies, we changed the regions that controlled the BMI between and within training sessions: meaning that animals could not rely on a habitual activity pattern or strategy, but had to continually explore different neural patterns to achieve reward on different training days. Animals did so by 'exploring' with highly variable neural activity patterns early in a training session, until they discovered a successful activity pattern they could reliably exploit (Figure 2). Target hit rates dropped when reward was dispensed randomly, unlinked to the target zone, indicating the animals' task performance was goal-directed, and not habitual.

Animals could arbitrarily decorrelate normally correlated brain areas during task execution, even though spontaneous activity was widely correlated across cortex in mice not performing the task, in agreement with previous work (Ledochowitsch et al., 2013). We found this to be true of both anterior and posterior cortical areas—in mice trained to control an auditory cursor, for example, posterior visual control areas could also be decorrelated during the task. However, animals performed better when control regions were less spontaneously correlated. Pupil and locomotion also became significantly decorrelated during task performance, indicating that task-engagement and locomotion may engage distinct arousal

mechanisms (Supp. Figure 8, (Vinck et al., 2015; Reimer et al., 2016; Clancy et al., 2019)).

By imaging dorsal cortex as animals performed this task, we were able to screen for cortical areas involved in expert BMI control. On the first day of training, V1 was most active during the task, but as animals learned the task over days, higher visual areas, including AM, PM and RL, became more active. When the same stimuli were played back to animals in an open-loop fashion (e.g. not controlled by animals), activation was again mainly evident in V1, suggesting these higher areas were involved in the goal-directed aspect of task performance. AM and RL are rodent homologues of parietal cortex (Glickfeld and Olsen, 2017; Wang et al., 2011), which has been shown in humans to be involved in intention and monitoring the mapping between action and outcome (Andersen and Buneo, 2002; Desmurget et al., 2009; Andersen and Cui, 2009; Aflalo et al., 2015; Cui, 2016). However, it was unclear whether the recruitment of parietal cortex over learning was related to the fact that it's involved with sensorimotor transformations generally, or because it's involved more specifically in planning and intentional control.

In order to clarify the role of parietal cortex in causal control, we recorded from individual neurons in a parietal area as animals performed a BMI task. We targeted extracellular recordings in one of the identified task-active areas, AM, to probe task-related changes in the spiking of single units. We found that units were more active during task performance than during passive playback of the same stimuli. In particular, units were more responsive to the target, and target-adjacent, stimuli during task performance compared to passive playback, similar to spatial attention boosting evident in previous work (Moran and Desimone, 1985; Engel et al., 2016), and in accordance with evidence that attention can reshape stimulus representations in a manner that more effectively guides decisions (Ruff and Cohen, 2019). This boosting did not appear to be simply reward expectation, and the animal did not use saccades or overt movements to perform the task. This boosting was also sensitive to the task goal: if the cursor was positioned close to

the target and sweeping towards it, responses were boosted relative to when it was sweeping away. If the cursor was far from the target and sweeping farther away from it, responses were also boosted relative to the cursor at the same position sweeping towards the target. This suggests that firing rates reflect intention, and may also reflect a valence of the animal's perceived fluency of cursor control—that is, whether it was successfully or unsuccessfully guiding the cursor towards its intended goal (Lee and Dan, 2012).

We present a novel task and imaging method for exploring the encoding of action-outcome assessments, which allowed us to simultaneously monitor–with both dorsal cortex-wide and cell-level resolution–what activity patterns support the causal control of external objects. While using widefield imaging afforded us a view of the dorsal cortex as animals learned neuroprosthetic control, there are a number of limitations to this method. Cortical neuroprosthetic control requires interactions with basal ganglia (Koralek et al., 2012; Neely et al., 2018), from which we cannot record using this method. Furthermore, we know from work in humans that prefrontal cortex (PFC) is involved in the sense of control over external stimuli, but we cannot record signals from PFC using this preparation due to its obscuration by the frontal sinus. While we found increased spiking to target stimuli using this preparation, we don't know the exact cellular or neuromodulatory mechanisms giving rise to this difference. Future work may address this by using mesoscale 2-photon imaging to record from molecularly defined neural subpopulations in parietal and motor control areas during task performance.

Acknowledgements

The authors would like to thank Adrianne Zhong for help with the camera control code, Ivana Orsolic for help with the widefield setup, Lisa Hoermann for performing surgeries for this project, and Sonja Hofer, Petr Znamenskiy, Spencer Wilson, Alex Naka, and Adrei Khilkevich for manuscript feedback and discussions of this work. This work was supported by the European Research Council (NeuroV1sion

616509 to T.D.M-F.), Swiss National Science Foundation (SNSF 31003A_169802 to T.D.M.- F.), the Wellcome Trust (090843/E/09/Z core grant to the Sainsbury Wellcome Centre), the EMBO Long-term Fellowship (ALTF 1481-2014 to K.B.C.), the HFSP Postdoctoral Fellowship (LT000414/2015-L to K.B.C.), and the Branco Weiss-Society in Science grant (K.B.C.).

Author contributions

K.B.C. planned and executed the experiments and analysed the data. K.B.C. and T.D.M.- F. wrote the manuscript.

Competing financial interests statement

The authors declare no competing financial interests.

Methods

All experimental procedures were carried out in accordance with institutional animal welfare guidelines and licensed by the Swiss cantonal veterinary office. TRE-Gcamp6s mice (Wekselblatt et al., 2016) (Jackson laboratories, https://www.jax.org/strain/024742) were crossed with B6.CBA-Tg(Camk2a-tTA)1Mmay/DboJ mice (Jackson laboratories, JAX 007004), to drive the expression of gCamp6s in CamKII+ pyramidal neurons. Animals were housed in a facility using a reversed light cycle, and recordings were taken during their active period. Eleven female mice were trained on the task, and we took electrophysiological recordings from seven of these, ranging between P55-P75. Sample sizes were not statistically determined, but were consistent with previous papers using related methodology (Clancy et al., 2019; Xiao et al., 2017).

Surgery

A week before training, mice were prepared for imaging. Animals were anaesthetised with a mixture of fentanyl (0.05 mg per kg), midazolam (5.0 mg per kg), and medetomidine (0.5 mg per kg). The animal's scalp was resected and a head plate was secured to the skull. Four stereotaxically placed marks were made to enable alignment of the imaged brain with the Allen Brain Atlas (http://mouse.brain-map.org/static/atlas) post hoc, using the Allen Brain API (brain-map.org/api/index.html). The exposed skull was cleaned and covered with transparent dental cement to avoid infection, and to cover the cut scalp edges (C&B Metabond). This was polished to enhance the transparency of the preparation. A custom-made 3D printed light shield was cemented to the skull and head plate to avoid light leaks from the visual stimulus.

Behavioral setup and recordings

The recording chamber was sound-isolated and shielded from outside light. Mice were head-fixed under the microscope and free to run on a Styrofoam running wheel (diameter = 20 cm, width = 12 cm). The animals' movements were recorded

using a rotary encoder in the wheel axis (pulse rate 1000, Kubler). Two monitors were placed side by side in front of the mouse, angled towards one another (21.5" monitors, ~20 cm from mouse, covering ~100x70 degrees of visual space), similarly to the setup described in (Poort et al., 2015). A reward port was place in front of the animal, where reward delivery was triggered via pinch solenoid (NResearch) and animal licks were detected using a custom piezo element coupled to the spout. All behavioral data were recorded using custom MATLAB software and a PCI-6320 acquisition board (National Instruments).

On electrophysiological recording days, pupil recordings were taken by illuminating the animal's right eye with a custom IR-light source and imaging with a CMOS camera (DMK22BUC03, Imaging Source, 30 Hz) using custom MATLAB software. Pupil size was determined as described in (Orsolic et al., 2019): images were first smoothed with a 2-D gaussian filter and thresholded to low luminance areas. These thresholded regions were then filtered by circularity and size to automatically detect the pupil region. Pupil edges were detected using the canny method, and ellipses were iteratively fit to the region, tasked to minimise the geometric distance between the area outline and the fit ellipse using nonlinear least squares (MATLAB function fitellipse, Richard Brown). The pupil diameter was taken to be the major axis of the ellipse, then normalised by animal. Pupil recordings from one animal had to be discarded, as the video was not sufficiently in focus.

Behavioral training

After recovery, mice were acclimatised to head fixation for a minimum of two days, and started on food restriction. Awake animals were head-fixed under the microscope and free to run on a Styrofoam wheel. A baseline of spontaneous activity was taken on every training day (10-20 minutes) in order to estimate spontaneous hit rates. The decoder was calibrated such that animals achieved ~25% performance on their first day. Two small control regions were chosen for real-time read out. The same control regions were used for the first few days of

training, then changed from day to day, or within sessions, so that animals did not learn a fixed control strategy.

Activity was imaged at 40 Hz and the mean fluorescence from each control region was transmuted to the cursor's position on screen with a simple transform:

$$p(t) = A_1 F_{R1} - A_2 F_{R2} + B$$

where p is the cursor position, F_{R1} and F_{R2} are the fluorescence of control regions one and two, respectively, and A_1, A_2 and B are coefficients set based on the daily spontaneous baseline recordings (minimum 10 minutes). The display updated at approximated 10 Hz, with a latency of 300 ms from camera to screen, measured using a photodiode placed on one of the monitors (Thorlabs, PDA100A-EC). The raw fluorescence was converted to $\Delta F/F$ using a moving baseline of 5 minutes of activity. Activity in R1 would cause the cursor to move towards the target location in the centre of the animal's visual field, while increased activity in R2 would cause the cursor to move away from the target. The cursor was presented on two monitors so that the animal could track the cursor with both eyes; its goal was to bring the cursors together in the middle of its visual field. These changes were binned, such that the cursor could take one of eight possible locations on the screen. The cursor had to be held at the target position for 0.3 seconds to count as a hit, at which point the cursor disappeared. When a target was hit, a MATLAB-controlled Data Acquisition board (National Instruments, Austin, TX) triggered the administration of a soyamilk reward following a 1 second delay. The next trial could be initiated within 5 seconds of reward delivery, but only when the activation of R1 relative to R2 returned to the mean value recording during spontaneous activity (to ensure enough time had passed for large transients to decay). If the animal did not bring the cursor to the target within a 30 second trial, the cursor disappeared, and the animal received a white noise tone and a 10 second 'time out.'

We trained a separate group of four mice using an auditory, rather than visual, feedback cursor, where activity was transmuted to the pitch of a feedback tone (Clancy et al., 2014). As with the visual feedback task, a spontaneous baseline

was recorded every day (10-20 minutes) to assess chance levels of performance and calibrate the decoder. Activity from two arbitrarily chosen regions was entered into an online transform algorithm that related neural activity to the pitch of an auditory cursor:

$$f(t) = A_1 e^{F_{R1}1} - A_2 e^{RF_{R2}} + B$$

Where f is the cursor frequency, F_{R1} is the fluorescence of R1, F_{R2} the fluorescence of R2, and A1, A2, and B are coefficients set based on the daily baseline recording. Linear changes in firing rate resulted in exponential changes in cursor frequency, and frequency changes were binned in quarter-octave intervals to match rodent psychophysical discrimination thresholds. As with the visual task, a trial was marked incorrect if the target pitch was not achieved within 30 seconds of trial initiation. The auditory feedback was played using speakers mounted on 2 sides of the imaging platform.

Widefield imaging

Widefield imaging was performed through the intact skull using a custom-built epifluorescence macroscope with photographic lenses in a face-to-face configuration (85mm f/1.8D objective, 50mm f/1.4D tube lens; (Ratzlaff and Grinvald, 1991)). Data were recorded using a CMOS camera (Pco.edge 5.5, PCO, Germany) in global shutter mode. 16-bit images were acquired at a rate of 40 Hz and binned 2x2 online using custom-made LABVIEW software. A constant illumination at 470 nm was provided (M470L3, Thorlands, excitation filter FF02-447/60-25), with average power ~0.05 mW.mm2 (emission filter 525/50-25, Semrock). The imaging site was shielded from light contamination using a 3D-printed blackout barrier glued to the animal's skull. Signals from the two control regions were sent via UDP to a computer providing visual or auditory feedback to the mouse, using custom MATLAB software.

Electrophysiological recordings

The day before recording, mice were anesthetised with isofluorane and a small craniotomy was opened over AM, which was functionally identified during task performance, and stereotaxically confirmed. The craniotomy was kept damp with Ringer's solution and sealed with KwikSil (World Precision Instruments). Recordings were taken on the following day to avoid residual effects of anesthesia.

On the recording day, animals were head-fixed under a custom-built widefield microscope, the skull and cortex was cleaned with Ringer's solution, and the KwikSil plug removed from the craniotomy. A custom-designed silicon probe (64 channels, 2 shanks, Neuronexus, as described in (Clancy et al., 2019)) was inserted at an angle of ~45 degrees from normal to cortex. The probe consisted of two shanks with 64 sites total, organised into 16 'tetrodes', each consisting of 4 sites located 25 um apart from each other within-tetrode, and tetrodes spaced 130 um apart from each other. A small amount of KwikSil or agar was used to cover the exposed cortex after the probe was in place. After allowing the probe to settle for 20-30 minutes, neural activity was recorded using the OpenEphys recording system (Siegle et al., 2017). Behavioral and stimulation data, including pulses representing each camera frame, were recorded using OpenEphys, enabling the alignment of electrophysiological signals with imaging and behavioral data. Ephys recordings were filtered between 700 and 7000 Hz, and spikes detected using the Klustakwik suite (Schmitzer-Torbert et al., 2005). Clusters were assigned to individual units by manual inspection, excluding any units without a clear refractory period. Units were separated into fast and broad spiking units by their peak-to-tough time, using a cutoff of 0.66 ms (Barthó et al., 2004).

Data analysis

Raw imaging data were checked for dropped frames, spatially binned 2x2, and loaded into MATLAB as a mapped tensor (Muir and Kampa, 2015). The raw fluorescence was converted to $\Delta F/F$ using a moving baseline, calculated as the tenth percentile of points from the preceding 20 seconds of data. We did not perform hemodynamic correction as previous work indicates that hemodynamic

and flavoprotein signals contribute minimally compared to the calcium responses (Vanni and Murphy, 2014; Xiao et al., 2017; Clancy et al., 2019).

Task-activation maps were calculated by taking the normalised average of fluorescence movies during the task, or visual stimulus, subtracted by periods when animals were not performing the task. To ensure that differences between early and late in training were not influenced by possible differences in the statistics of the visual feedback cursor, we randomly excluded success trials on late training days in order to have comparable numbers of success and failure trials between early and late training. To build the single-unit affiliation maps (Supp. Figure 9, see also (Clancy et al., 2019)), spike trains were binned to match imaging frames, and maps were calculated by taking the correlation of each unit's spike train with each pixel's $\Delta F/F$.

Spectral entropy was calculated in 10 second windows, each overlapping by 5 seconds. The calcium signal of the control areas was transformed into power spectral density (PSD) during these windows (the magnitude squared of the signal's Fourier transform). This was then used to calculate the spectral entropy for that time span:

$$SE = -\sum_{f=\frac{-f_s}{2}}^{f=\frac{f_s}{2}} PSD_n(f) log_2[PSD_n(f)]$$

Where SE is the spectral entropy, PSD_n is the normalised PSD, and *f* is frequency.

The data and code used in this study are available from the corresponding author upon reasonable request.

References

Aflalo, T., Kellis, S., Klaes, C., Lee, B., Shi, Y., Pejsa, K., Shanfield, K., Hayes-Jackson, S., Aisen, M., Heck, C., et al. (2015). Neurophysiology. Decoding motor imagery from the posterior parietal cortex of a tetraplegic human. Science *348*, 906–910.

Andersen, R.A., and Buneo, C.A. (2002). Intentional maps in posterior parietal cortex. Annu. Rev. Neurosci. *25*, 189–220.

Andersen, R.A., and Cui, H. (2009). Intention, Action Planning, and Decision Making in Parietal-Frontal Circuits. Neuron *63*, 568–583.

Andersen, R.A., Snyder, L.H., Bradley, D.C., and Xing, J. (1997). Multimodal representation of space in the posterior parietal cortex and its use in planning movements. Annu. Rev. Neurosci. *20*, 303–330.

Bagur, S., Averseng, M., Elgueda, D., David, S., Fritz, J., Yin, P., Shamma, S., Boubenec, Y., and Ostojic, S. (2018). Go/No-Go task engagement enhances population representation of target stimuli in primary auditory cortex. Nat. Commun. *9*, 2529.

Bakay, R.A.E., and Kennedy, P.R. (1998). Cognitive Engineering: Proof of Principle. Neurosurgery *43*, 706–706.

Barson, D., Hamodi, A.S., Shen, X., Lur, G., Constable, R.T., Cardin, J., Crair, M., and Higley, M. (2018). Simultaneous mesoscopic and two-photon imaging of neuronal activity in cortical circuits. BioRxiv 468348.

Barthó, P., Hirase, H., Monconduit, L., Zugaro, M., Harris, K.D., and Buzsáki, G. (2004). Characterization of Neocortical Principal Cells and Interneurons by Network Interactions and Extracellular Features. J. Neurophysiol. *92*, 600–608.

Carmena, J.M., Lebedev, M.A., Crist, R.E., O'Doherty, J.E., Santucci, D.M., Dimitrov, D.F., Patil, P.G., Henriquez, C.S., and Nicolelis, M.A.L. (2003). Learning to Control a Brain–Machine Interface for Reaching and Grasping by Primates. PLOS Biol. *1*, e42.

Chambon, V., Moore, J.W., and Haggard, P. (2015). TMS stimulation over the inferior parietal cortex disrupts prospective sense of agency. Brain Struct. Funct. *220*, 3627–3639.

Clancy, K.B., Koralek, A.C., Costa, R.M., Feldman, D.E., and Carmena, J.M. (2014). Volitional modulation of optically recorded calcium signals during neuroprosthetic learning. Nat. Neurosci. *17*, 807–809.

Clancy, K.B., Orsolic, I., and Mrsic-Flogel, T.D. (2019). Locomotion-dependent remapping of distributed cortical networks. Nat. Neurosci.

Collinger, J.L., Wodlinger, B., Downey, J.E., Wang, W., Tyler-Kabara, E.C., Weber, D.J., McMorland, A.J., Velliste, M., Boninger, M.L., and Schwartz, A.B. (2013). High-

performance neuroprosthetic control by an individual with tetraplegia. The Lancet *381*, 557–564.

Cui, H. (2016). Forward Prediction in the Posterior Parietal Cortex and Dynamic Brain-Machine Interface. Front. Integr. Neurosci. 10:35.

Desmurget, M., Reilly, K.T., Richard, N., Szathmari, A., Mottolese, C., and Sirigu, A. (2009). Movement intention after parietal cortex stimulation in humans. Science *324*, 811–813.

Dewey, J. (1896). The reflex arc concept in psychology. Psychol. Rev. *3*, 357–370.

Donoghue, J.P. (2002). Connecting cortex to machines: recent advances in brain interfaces. Nat. Neurosci. *5 Suppl*, 1085–1088.

Engel, T.A., Steinmetz, N.A., Gieselmann, M.A., Thiele, A., Moore, T., and Boahen, K. (2016). Selective modulation of cortical state during spatial attention. Science *354*, 1140–1144.

Fetz, E.E. (1969). Operant conditioning of cortical unit activity. Science *163*, 955–958.

Glickfeld, L.L., and Olsen, S.R. (2017). Higher-Order Areas of the Mouse Visual Cortex. Annu. Rev. Vis. Sci. *3*, 251–273.

Haggard, P. (2017). Sense of agency in the human brain. Nat. Rev. Neurosci. *18*, 196–207.

Hochberg, L.R., Bacher, D., Jarosiewicz, B., Masse, N.Y., Simeral, J.D., Vogel, J., Haddadin, S., Liu, J., Cash, S.S., Smagt, P. van der, et al. (2012). Reach and grasp by people with tetraplegia using a neurally controlled robotic arm. Nature *485*, 372–375.

Kahnt, T., Park, S.Q., Haynes, J.-D., and Tobler, P.N. (2014). Disentangling neural representations of value and salience in the human brain. Proc. Natl. Acad. Sci. *111*, 5000–5005.

Koralek, A.C., Jin, X., Long, J.D., Costa, R.M., and Carmena, J.M. (2012). Corticostriatal plasticity is necessary for learning intentional neuroprosthetic skills. Nature *483*, 331–335.

Ledochowitsch, P., Koralek, A.C., Moses, D., Carmena, J.M., and Maharbiz, M.M. (2013). Sub-mm functional decoupling of electrocortical signals through closed-loop BMI learning. Conf. Proc. Annu. Int. Conf. IEEE Eng. Med. Biol. Soc. IEEE Eng. Med. Biol. Soc. Annu. Conf. *2013*, 5622–5625.

Lee, S.-H., and Dan, Y. (2012). Neuromodulation of brain states. Neuron *76*, 209–222.

Licata, A.M., Kaufman, M.T., Raposo, D., Ryan, M.B., Sheppard, J.P., and Churchland, A.K. (2017). Posterior Parietal Cortex Guides Visual Decisions in Rats. J. Neurosci. Off. J. Soc. Neurosci. *37*, 4954–4966.

Makino, H., Ren, C., Liu, H., Kim, A.N., Kondapaneni, N., Liu, X., Kuzum, D., and Komiyama, T. (2017). Transformation of Cortex-wide Emergent Properties during Motor Learning. Neuron *94*, 880-890.e8.

Mohan, H., Gallero-Salas, Y., Carta, S., Sacramento, J., Laurenczy, B., Sumanovski, L.T., Kock, C.P.J. de, Helmchen, F., and Sachidhanandam, S. (2018). Sensory representation of an auditory cued tactile stimulus in the posterior parietal cortex of the mouse. Sci. Rep. *8*, 7739.

Moran, J., and Desimone, R. (1985). Selective attention gates visual processing in the extrastriate cortex. Science *229*, 782–784.

Muir, D.R., and Kampa, B. (2015). FocusStack and StimServer: A new open source MATLAB toolchain for visual stimulation and analysis of two-photon calcium neuronal imaging data. Front. Neuroinformatics *8*.

Neely, R.M., Koralek, A.C., Athalye, V.R., Costa, R.M., and Carmena, J.M. (2018). Volitional Modulation of Primary Visual Cortex Activity Requires the Basal Ganglia. Neuron *97*, 1356-1368.e4.

Nicolelis, M.A. (2001). Actions from thoughts. Nature *409*, 403–407.

Orsolic, I., Rio, M., Mrsic-Flogel, T.D., and Znamenskiy, P. (2019). Mesoscale cortical dynamics reflect the interaction of sensory evidence and temporal expectation during perceptual decision-making. BioRxiv 552026.

Peters, A.J., Steinmetz, N.A., Harris, K.D., and Carandini, M. (2019). Striatal activity reflects cortical activity patterns. BioRxiv.

Pho, G.N., Goard, M.J., Woodson, J., Crawford, B., and Sur, M. (2018). Task-dependent representations of stimulus and choice in mouse parietal cortex. Nat. Commun. *9*, 2596.

Pisella, L., Gréa, H., Tilikete, C., Vighetto, A., Desmurget, M., Rode, G., Boisson, D., and Rossetti, Y. (2000). An 'automatic pilot' for the hand in human posterior parietal cortex: toward reinterpreting optic ataxia. Nat. Neurosci. *3*, 729–736.

Poort, J., Khan, A.G., Pachitariu, M., Nemri, A., Orsolic, I., Krupic, J., Bauza, M., Sahani, M., Keller, G.B., Mrsic-Flogel, T.D., et al. (2015). Learning Enhances Sensory and Multiple Non-sensory Representations in Primary Visual Cortex. Neuron *86*, 1478–1490.

Prsa, M., Galiñanes, G.L., and Huber, D. (2017). Rapid Integration of Artificial Sensory Feedback during Operant Conditioning of Motor Cortex Neurons. Neuron *93*, 929-939.e6.

Ratzlaff, E.H., and Grinvald, A. (1991). A tandem-lens epifluorescence macroscope: hundred-fold brightness advantage for wide-field imaging. J. Neurosci. Methods *36*, 127–137.

Reimer, J., McGinley, M.J., Liu, Y., Rodenkirch, C., Wang, Q., McCormick, D.A., and Tolias, A.S. (2016). Pupil fluctuations track rapid changes in adrenergic and cholinergic activity in cortex. Nat. Commun. *7*, 13289.

Ruff, D.A., and Cohen, M.R. (2019). Simultaneous multi-area recordings suggest that attention improves performance by reshaping stimulus representations. Nat. Neurosci. *22*, 1669–1676.

Sadtler, P.T., Quick, K.M., Golub, M.D., Chase, S.M., Ryu, S.I., Tyler-Kabara, E.C., Yu, B.M., and Batista, A.P. (2014). Neural constraints on learning. Nature *512*, 423–426.

Schmitzer-Torbert, N., Jackson, J., Henze, D., Harris, K., and Redish, A.D. (2005). Quantitative measures of cluster quality for use in extracellular recordings. Neuroscience *131*, 1–11.

Serruya, M.D., Hatsopoulos, N.G., Paninski, L., Fellows, M.R., and Donoghue, J.P. (2002). Instant neural control of a movement signal. Nature *416*, 141–142.

Siegle, J.H., Cuevas López, A., Patel, Y., Abramov, K., Ohayon, S., and Voigts, J. (2017). Open Ephys: An open-source, plugin-based platform for multichannel electrophysiology. J. Neural Eng.

Sitaram, R., Caria, A., Veit, R., Gaber, T., Rota, G., Kuebler, A., and Birbaumer, N. (2007). fMRI Brain-Computer Interface: A Tool for Neuroscientific Research and Treatment. Comput. Intell. Neurosci. *2007*.

Sitaram, R., Ros, T., Stoeckel, L., Haller, S., Scharnowski, F., Lewis-Peacock, J., Weiskopf, N., Blefari, M.L., Rana, M., Oblak, E., et al. (2017). Closed-loop brain training: the science of neurofeedback. Nat. Rev. Neurosci. *18*, 86–100.

Sugrue, L.P., Corrado, G.S., and Newsome, W.T. (2004). Matching behavior and the representation of value in the parietal cortex. Science *304*, 1782–1787.

Tervo, D.G.R., Proskurin, M., Manakov, M., Kabra, M., Vollmer, A., Branson, K., and Karpova, A.Y. (2014). Behavioral Variability through Stochastic Choice and Its Gating by Anterior Cingulate Cortex. Cell *159*, 21–32.

Trautmann, E.M., O'Shea, D.J., Sun, X., Marshel, J.H., Crow, A., Hsueh, B., Vesuna, S., Cofer, L., Bohner, G., Allen, W., et al. (2019). Dendritic calcium signals in rhesus macaque motor cortex drive an optical brain-computer interface. BioRxiv 780486.

Vanni, M.P., and Murphy, T.H. (2014). Mesoscale Transcranial Spontaneous Activity Mapping in GCaMP3 Transgenic Mice Reveals Extensive Reciprocal Connections between Areas of Somatomotor Cortex. J. Neurosci. *34*, 15931–15946.

Vinck, M., Batista-Brito, R., Knoblich, U., and Cardin, J.A. (2015). Arousal and locomotion make distinct contributions to cortical activity patterns and visual encoding. Neuron *86*, 740–754.

Wang, Q., Gao, E., and Burkhalter, A. (2011). Gateways of Ventral and Dorsal Streams in Mouse Visual Cortex. J. Neurosci. *31*, 1905–1918.

Weiskopf, N., Veit, R., Erb, M., Mathiak, K., Grodd, W., Goebel, R., and Birbaumer, N. (2003). Physiological self-regulation of regional brain activity using real-time functional magnetic resonance imaging (fMRI): methodology and exemplary data. NeuroImage *19*, 577–586.

Wekselblatt, J.B., Flister, E.D., Piscopo, D.M., and Niell, C.M. (2016). Large-scale imaging of cortical dynamics during sensory perception and behavior. J. Neurophysiol. *115*, 2852–2866.

Wisniewski, D., Reverberi, C., Momennejad, I., Kahnt, T., and Haynes, J.-D. (2015). The Role of the Parietal Cortex in the Representation of Task–Reward Associations. J. Neurosci. *35*, 12355–12365.

Xiao, D., Vanni, M.P., Mitelut, C.C., Chan, A.W., LeDue, J.M., Xie, Y., Chen, A.C., Swindale, N.V., and Murphy, T.H. (2017). Mapping cortical mesoscopic networks of single spiking cortical or sub-cortical neurons. ELife *6*.

Supplementary Information

The sensory representation of causally controlled objects

Kelly B. Clancy and Thomas D. Mrsic-Flogel

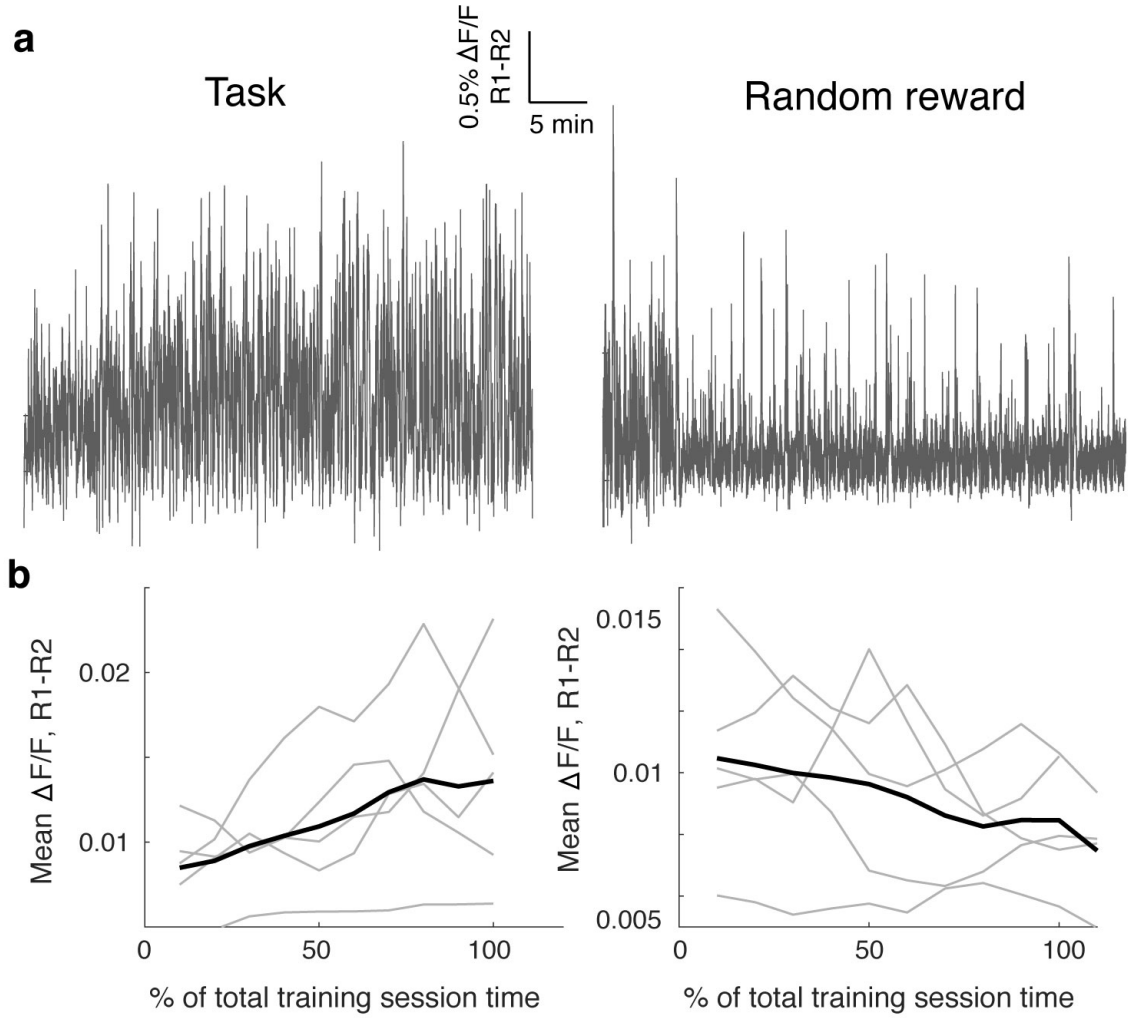

Supplementary Figure 1. Animals intentionally modulate activity patterns

a. Example trace of the difference between control areas' fluorescence during task (R1-R2), showing an increase in differential modulation over the course of a training session (left). These modulations decreased when reward was provided randomly (right). **b.** The slope of R1-R2 ΔF/F was positive during the normal task (left, $p < 0.01$, $n = 5$ mice) and negative over the course of random reward (right, $p < 0.01$, $n = 5$ mice).

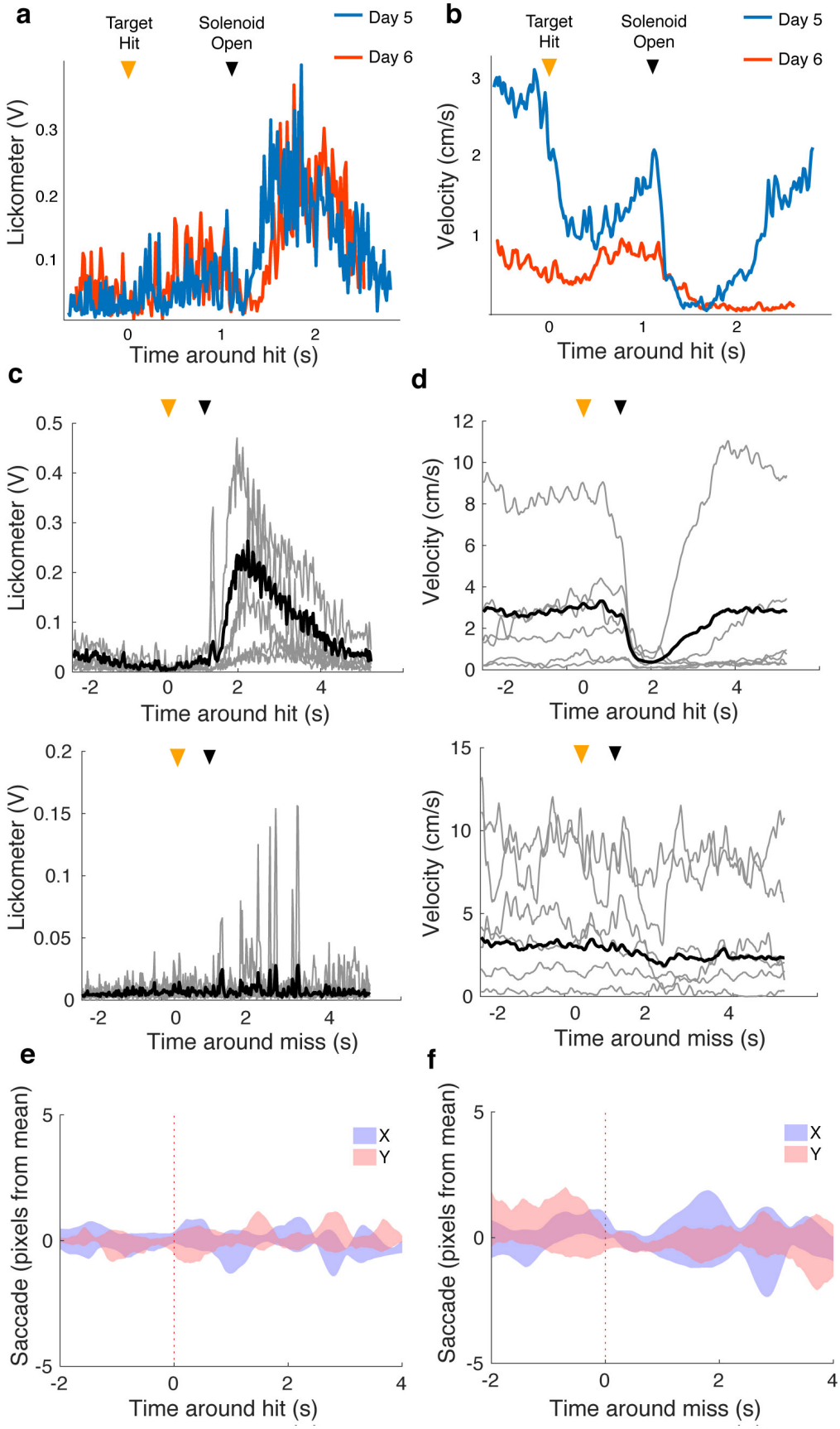
a
Target Hit
Solenoid Open
Day 5
Day 6
Lickometer (V)
Time around hit (s)
b
Velocity (cm/s)
Time around hit (s)
c
Lickometer (V)
Time around hit (s)
d
Velocity (cm/s)
Time around hit (s)
Lickometer (V)
Time around miss (s)
Velocity (cm/s)
Time around miss (s)
e
X
Y
Saccade (pixels from mean)
Time around hit (s)
f
Saccade (pixels from mean)
Time around miss (s)

Supplementary Figure 2. Animals did not use gross motor movements to perform task

a. Lick averaged around hits on 2 consecutive days of training for the same animal. **b.** Velocity averaged around hits on 2 consecutive days of training for the same animal. **c.** Lick averaged around hits (top) and misses (bottom) on day 8 of training (n = 7 mice). **d.** Velocity averaged around hits (top) and misses (bottom) on day 8 of training (n = 7 mice). **e.** Saccade averaged around hits, 95% confidence interval (n = 6 mice). **f.** Same as e, for misses (n = 6 mice).

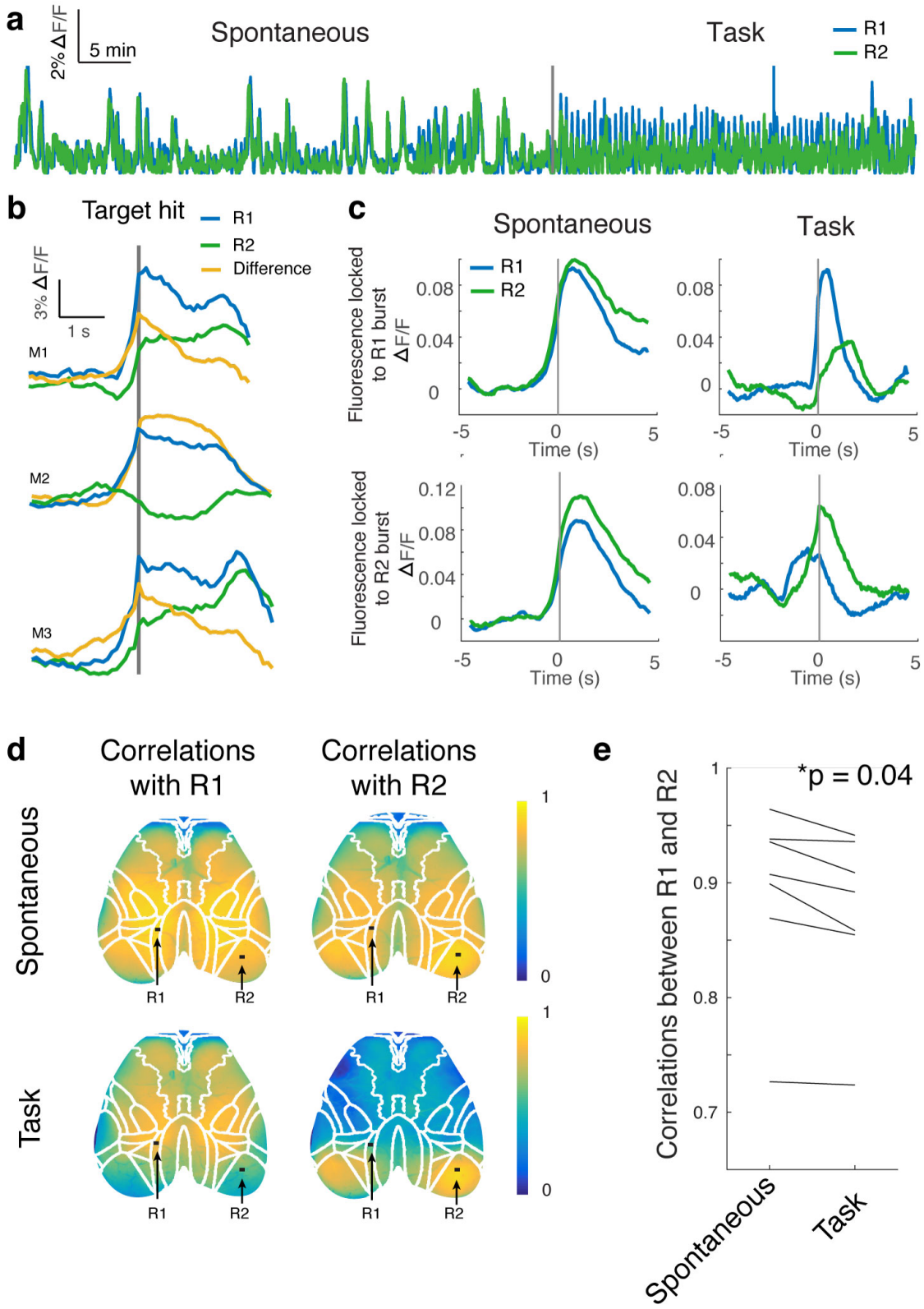

Supplementary Figure 3. Animals use different strategies to perform task

a. Example fluorescence trace from R1 and R2 in pre-task spontaneous activity, and during task. **b.** $\Delta F/F$ triggered around hits for three example animals, indicating different strategies animals use to achieve reward. **c.** $\Delta F/F$ triggered around large R1 transients (top) and R2 transients (bottom), before (left) and during (right) the training session, with the z-scored value of $\Delta F/F > 3$ as the threshold. **d.** Example correlation maps with R1 (left) or R2 (right) used as a seed pixel in spontaneous activity (top) vs during task performance (bottom), in an auditory-feedback based task. **e.** Correlations between R1 and R2 dropped between spontaneous activity and task performance (n = 7 mice, paired t-test).

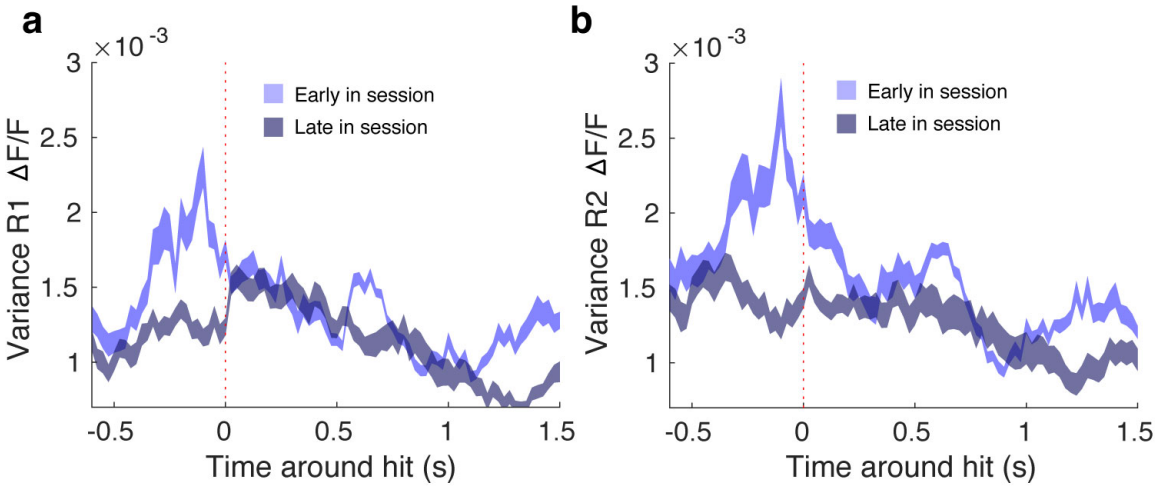

Supplementary Figure 4. Activity variance around hits decreased as animals discovered reliable strategies

a. Early in a training session, the average variance of activity in R1 was greater around hits than late in session (n = 7 mice, day 8 of training, shading indicates s.e.m.), indicating mice honed in on more reliable control strategies. **b.** Same as a, for R2.

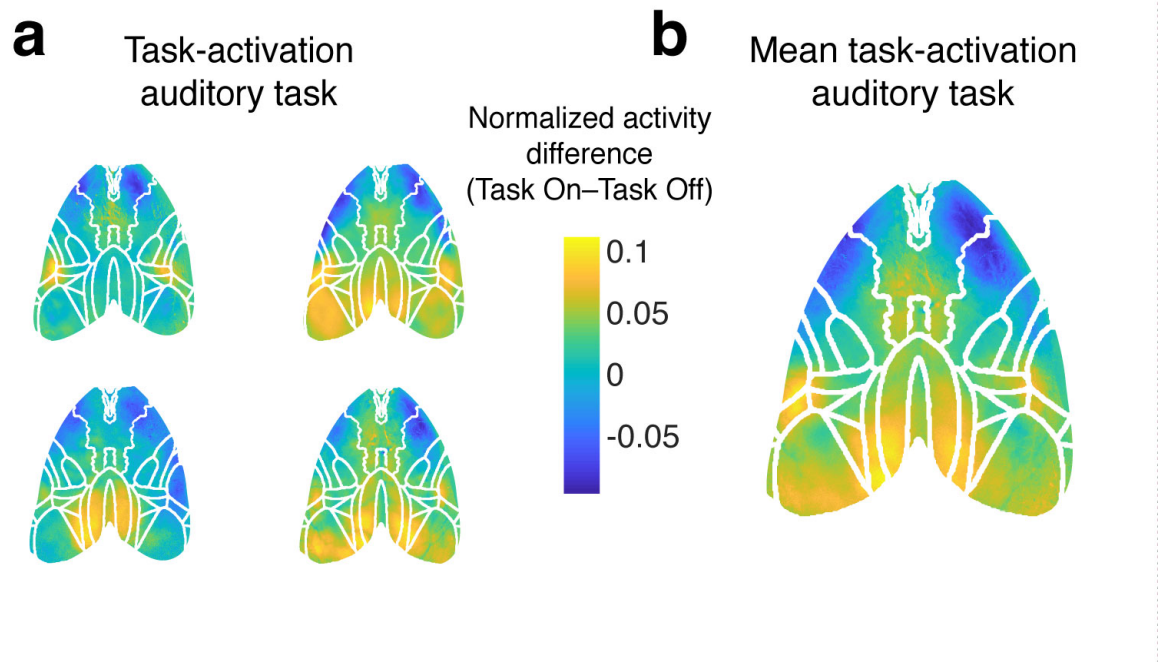

Supplementary Figure 5. Variable areas involved in auditory task

a. Example task-related activity maps from four animals trained on an auditory version of the task. **b.** Mean task-related activity map indicating involvement of lateral parietal homologue RL.

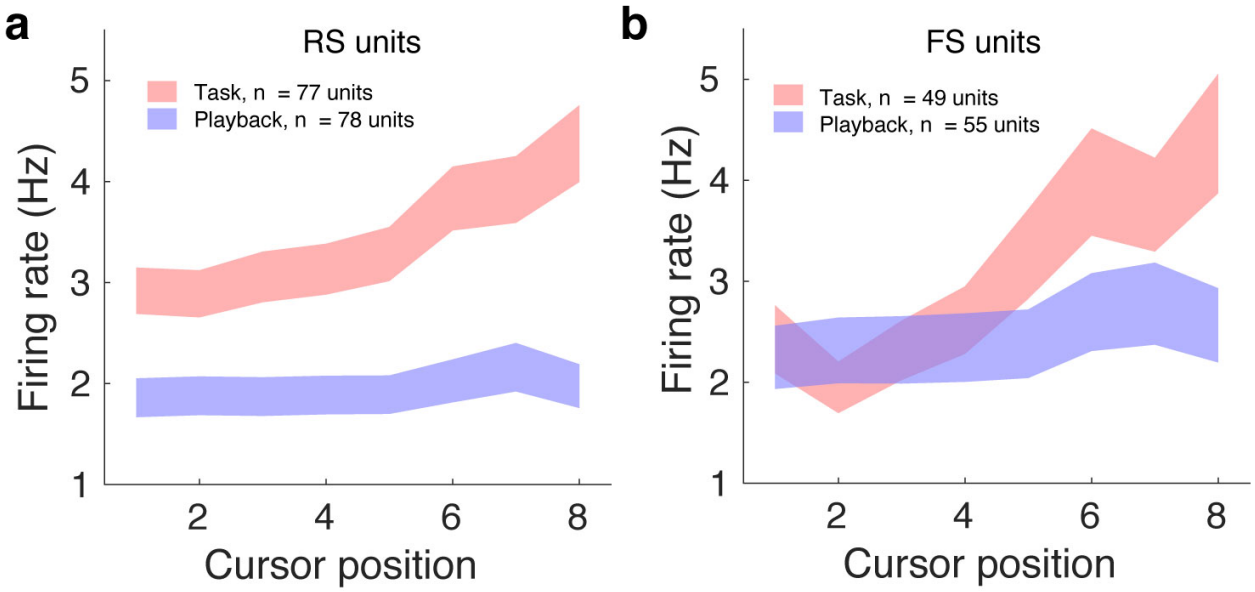

Supplementary Figure 6. Similar task-related tuning shifts for FS and RS units

a. Mean firing rate for RS units to different stimulus positions during task performance (95% confidence interval around mean indicated by shading, n = 7 mice). **b.** Same as **a**, for FS units.

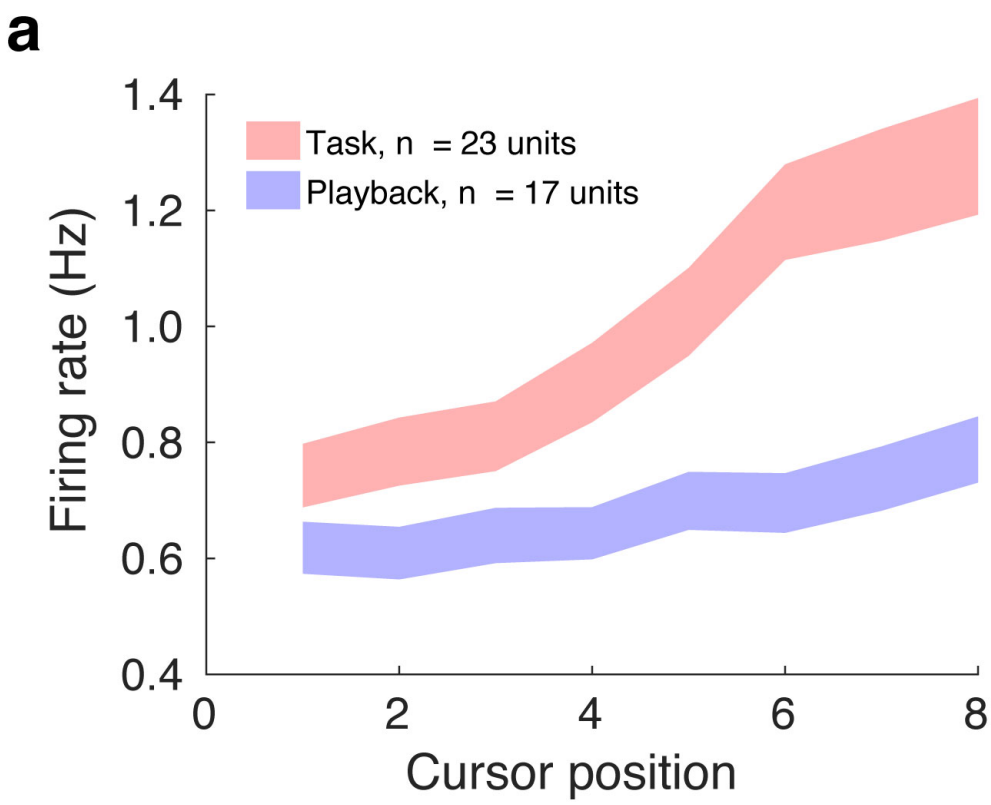

Supplementary Figure 7. Boosted firing rate at target position was not explained by reward expectation

a. Firing rates for units recorded in 2 animals where the target cursor position was rewarded during passive playback. The enhanced firing for target-adjacent stimuli during task performance remained, suggesting the boosting was not simply reward expectation (95% confidence interval around mean indicated by shading, n = 2 mice).

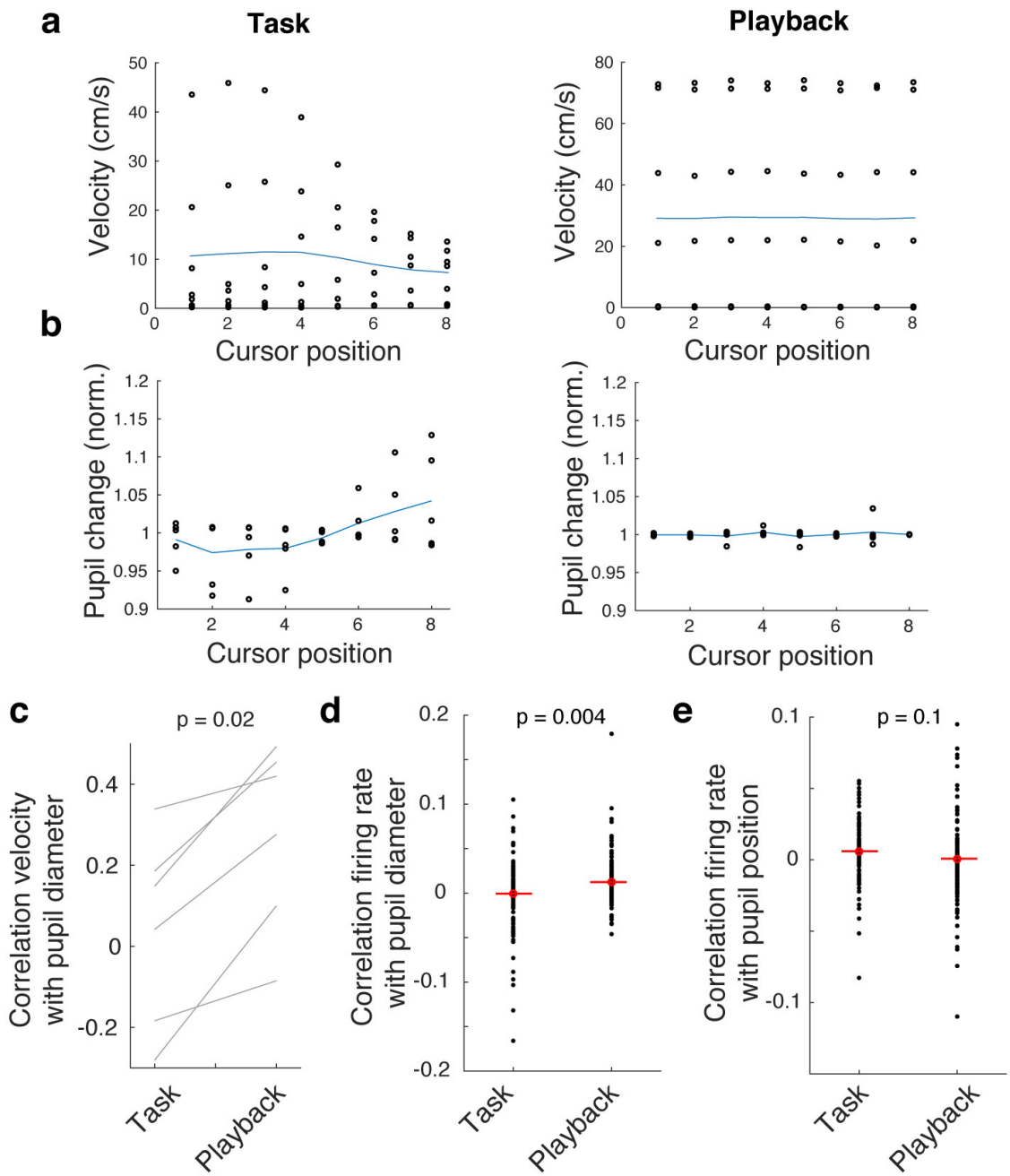

Supplementary Figure 8. Pupil and locomotion become uncoupled during task

a. Average velocity at each stimulus location during recordings during task (left) and playback (right), (n = 7 mice, final day of recording). **b**. Normalized pupil diameter at each stimulus location during task (left) and playback (right). **c.** Pupil diameter and running speed were significantly decorrelated during task performance compared to playback (n = 6 mice, paired t-test). **d.** The correlation

between firing rate and pupil diameter was not different from zero during task, but slightly higher during playback (reward periods and inter-trial intervals excluded, n = 6 mice, N = 105 units task, n= 122 units playback, t-test). **e.** Firing rate and pupil position were uncorrelated both during task and playback (reward periods and inter-trial intervals excluded, N = 6 mice, n = 105 units task, n = 122 units playback, t-test).

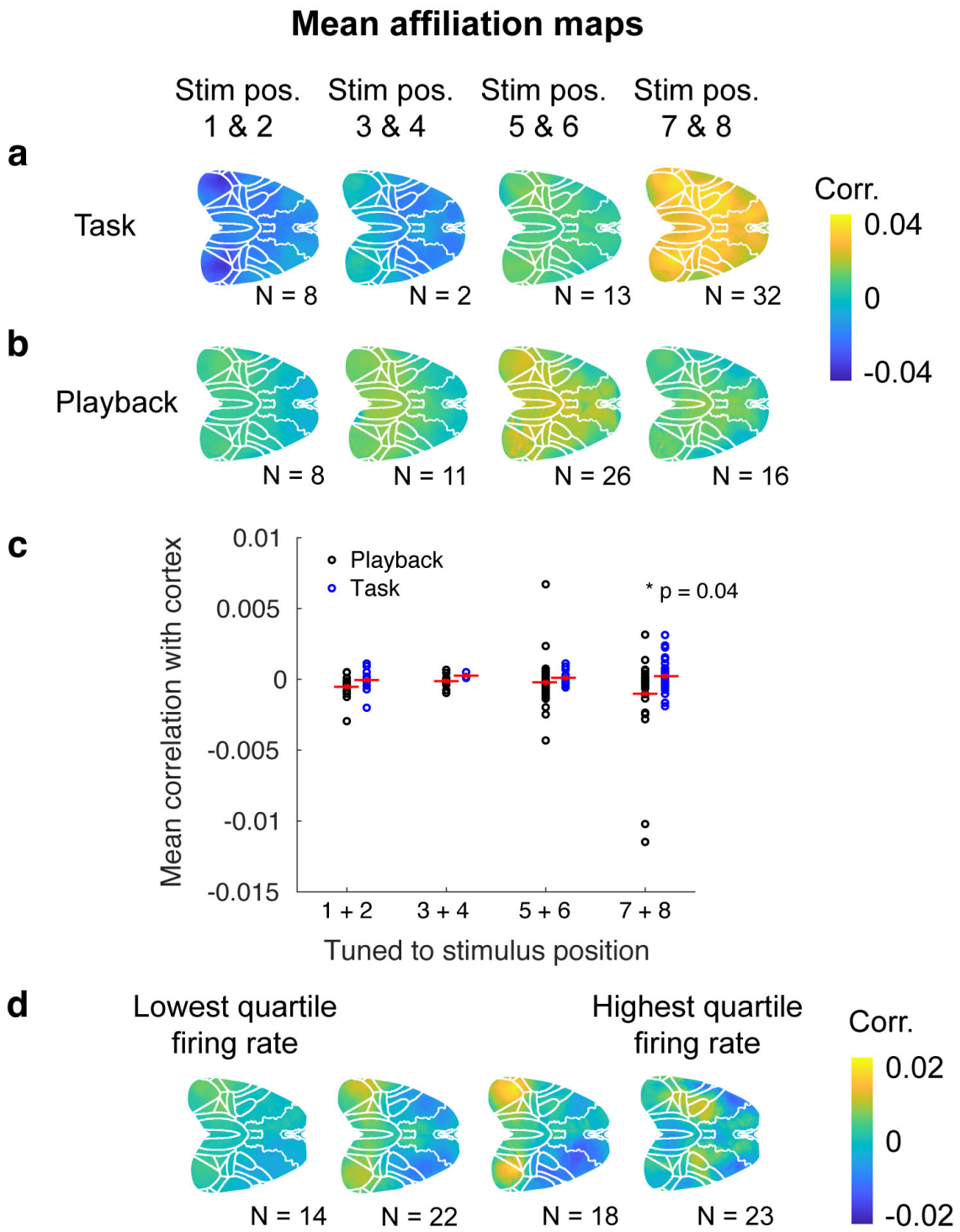

Supplementary Figure 9. Cortex-wide affiliations of units tuned to different stimuli

a. Spike trains for each unit were correlated with the activity of each pixel to build cortex-wide affiliation maps. These were sorted into bins based on which stimulus position units were most responsive to. The average of these maps is shown in **a** for task performance, and **b** for passive playback. **c.** Mean correlation of spiking activity with calcium activity across dorsal cortex, sorted by units' stimulus preference for task and playback (t-test, Bonferroni corrected). **d.** The trend seen in **a** is not due to higher firing rates of target stimulus-tuned units, when units were organized into quartiles of mean firing rates rather than stimulus preference.